Global View of Cosmic Ray Data

One Century Later
Triumph of the High Resolution Measurements

Serap Tilav
Bartol Research Institute
University of Delaware

When looked in detail the CR spectrum is not a boring simple power law

Direct Measurements
Satellite, Balloon

Indirect Measurements
Air Shower Experiments

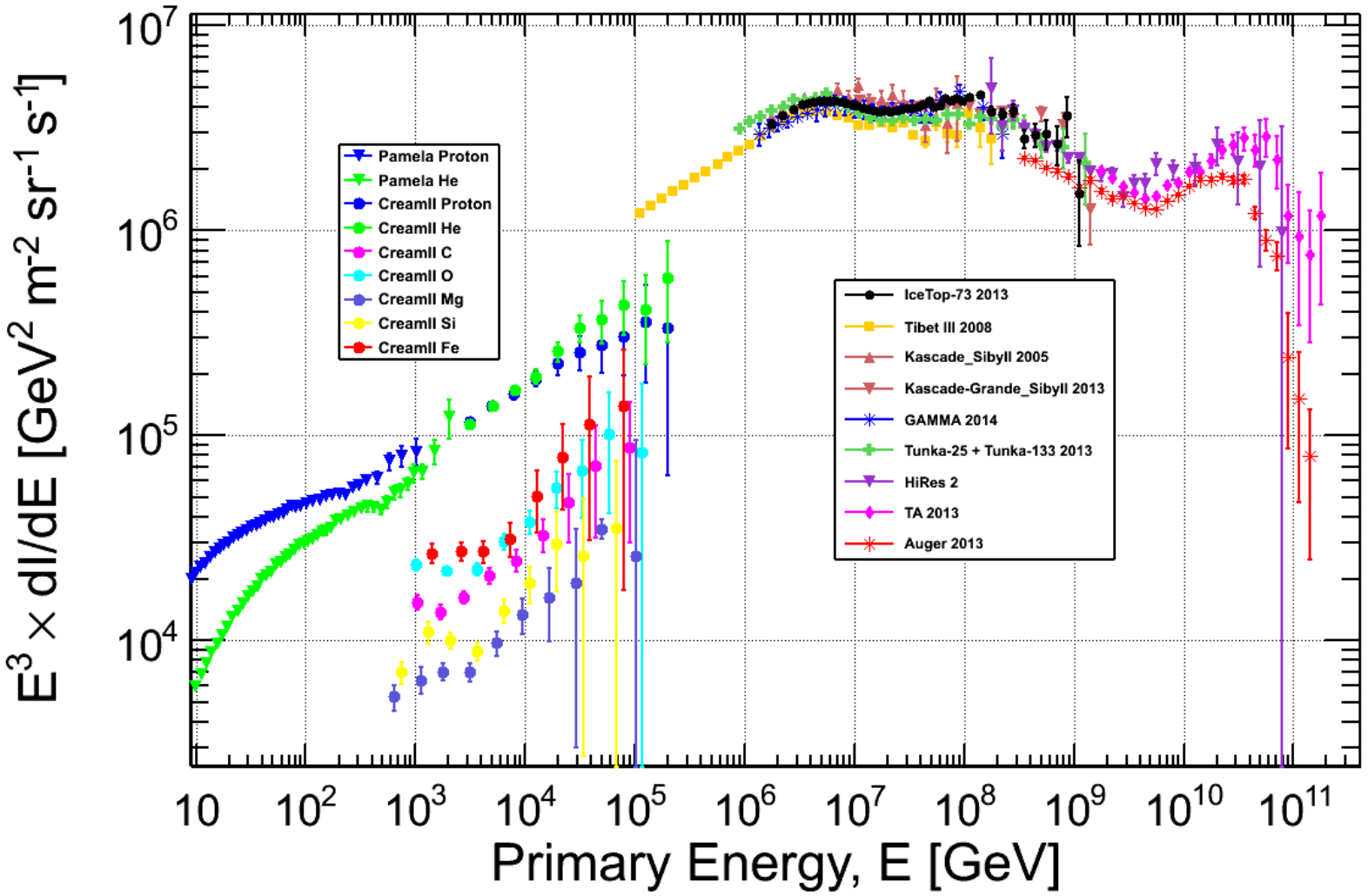

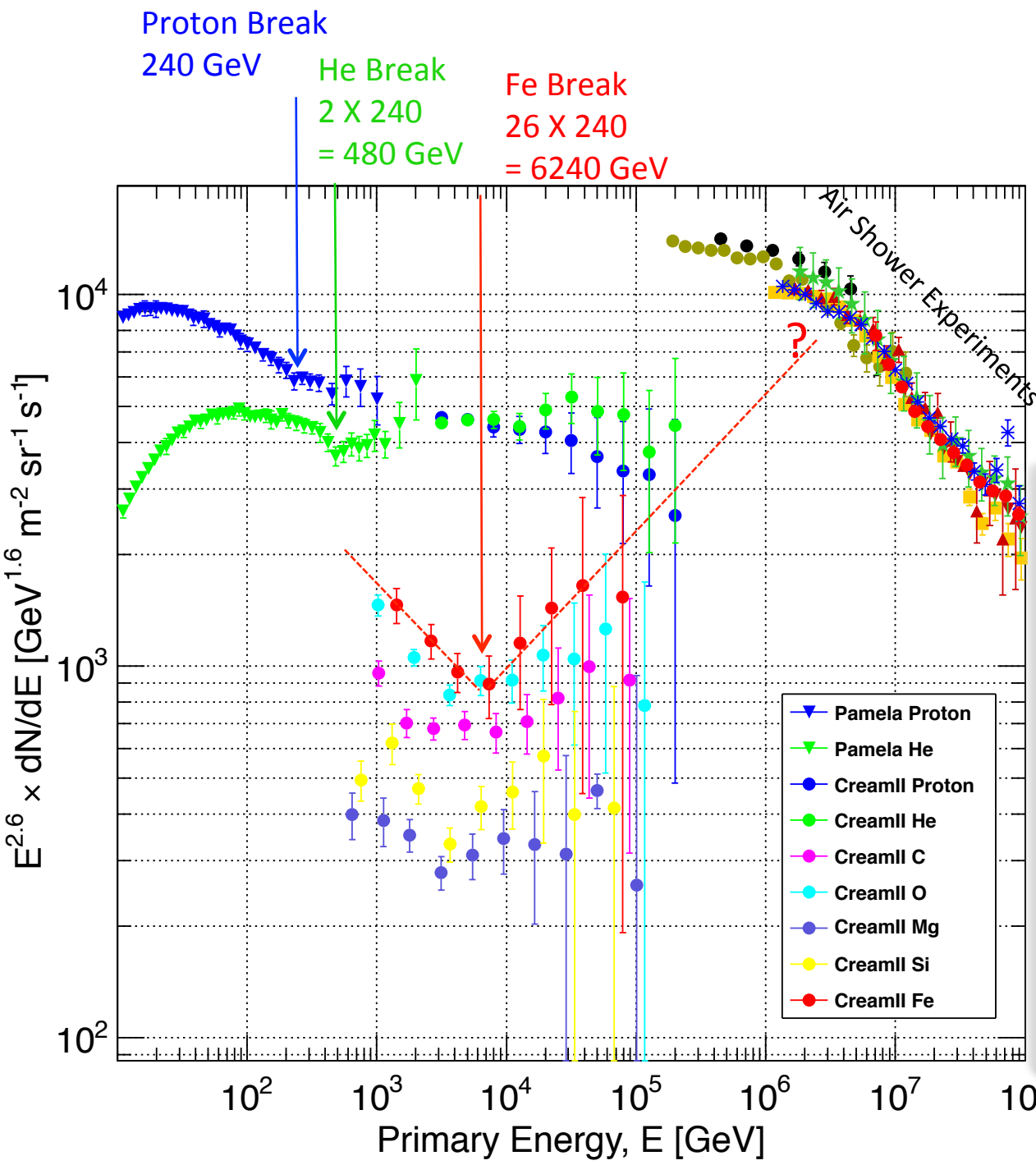

PAMELA /ATIC/ CREAM reveal rigidity dependent spectral breaks and remarkable hardening after the breaks

Perfect demonstration of Peters cycle:

When protons accelerated to E^{p}_{max} *a nucleus with Ze will be accelerated up to* $E^{z}_{max} = Ze \times R = Z \times E^{p}_{max}$

where magnetic rigidity $R = Pc/Ze$

Bernard Peters 1961

Spectral Indices of the hard component

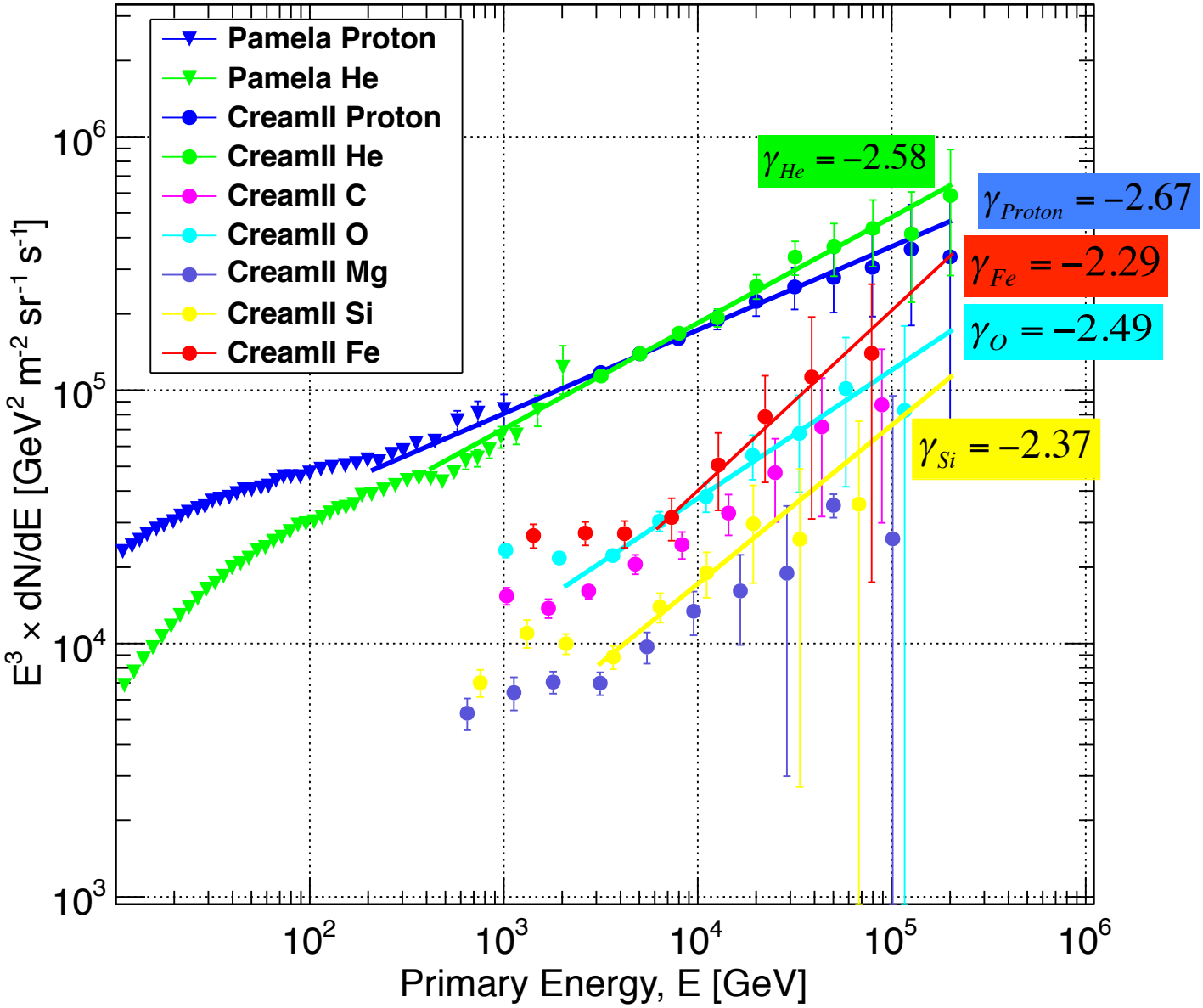

All Particle Spectrum from Air Shower Experiments

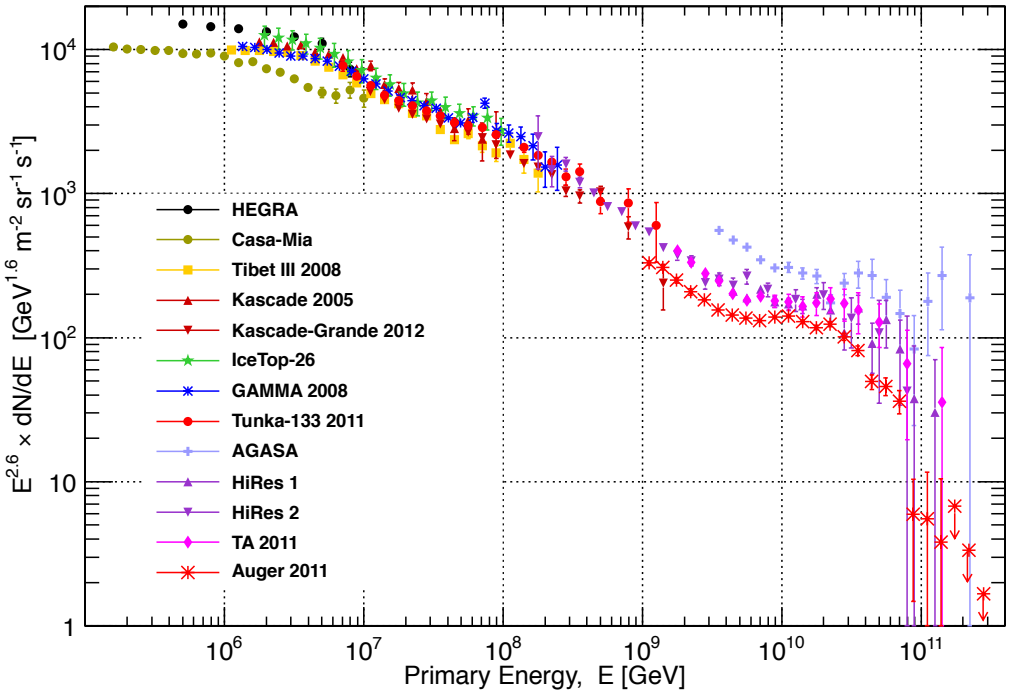

selection based on variety of techniques:

- cherenkov
- fluorescence
- scintillators
- muon counters

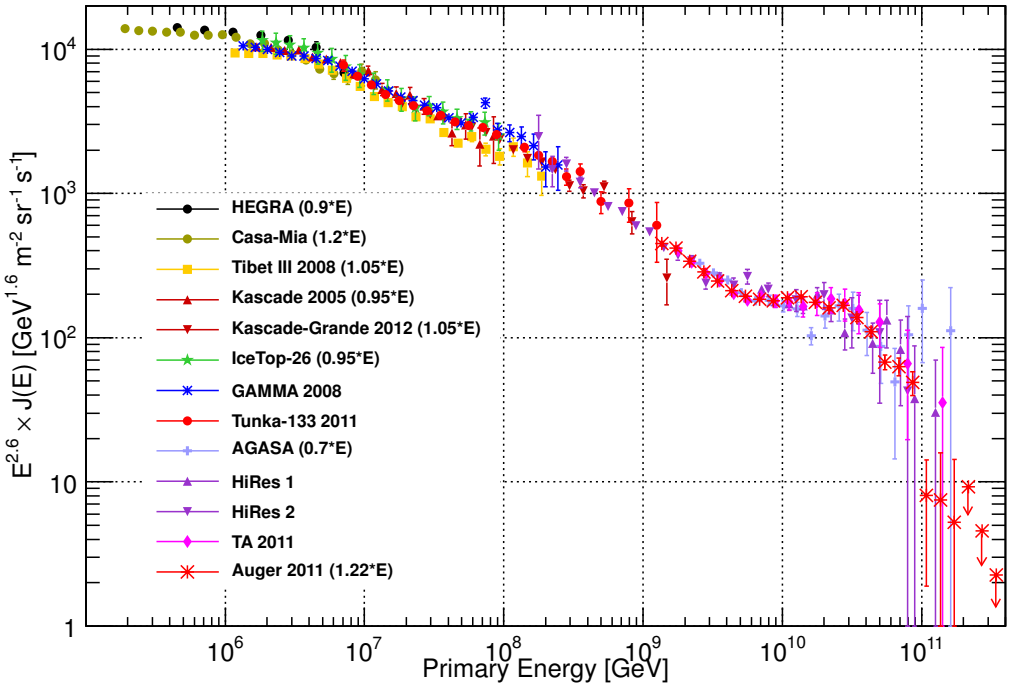

Gaisser's cross-calibrated spectrum:

5-20% energy shift to align features in the spectrum

arXiv:1303.3565 [astro-ph.HE] 14 Mar 2013
Gaisser , Stanev ,Tilav

The mean logarithmic mass <lnA> from Air Shower Experiments

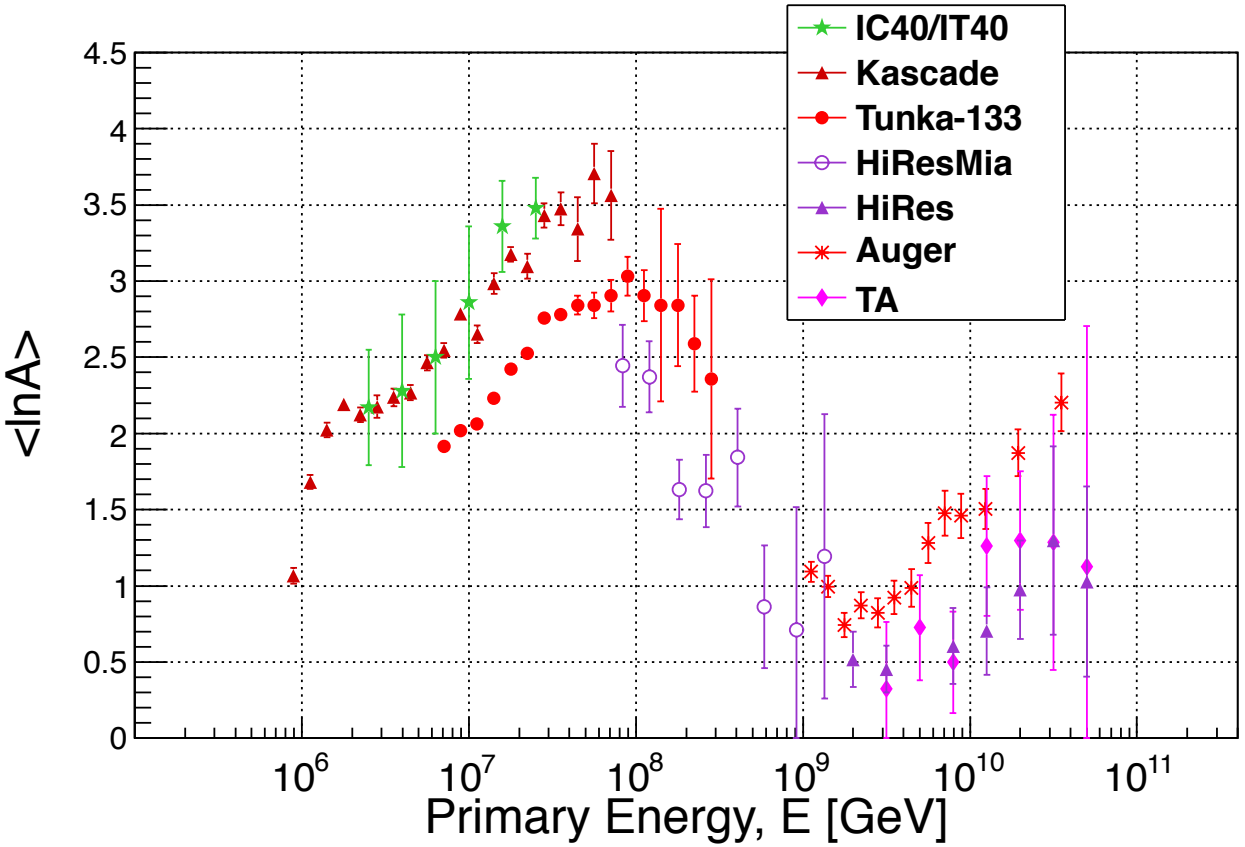

IC40/IT40, Tunka-133, Auger are published by the experiments

Kascade/HiRes/TA do not provide <lnA>

Use derived data by Kampert and Unger analysis

K. H. Kampert and M. Unger, Astropart. Phys., 2012, 35(10): 660

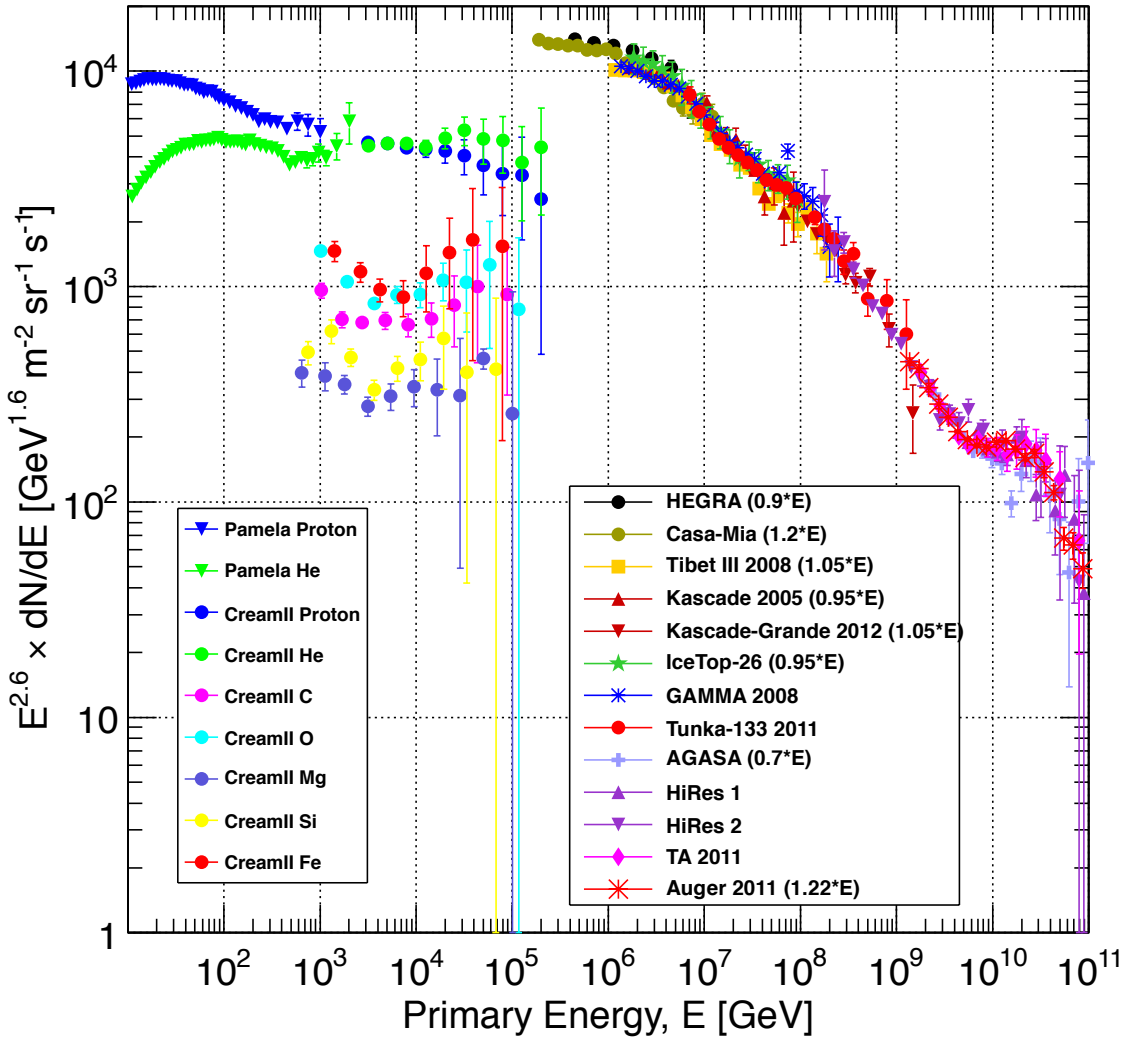

Fit the combined spectrum with Gaisser's formulation of Peters cycle

$$E\frac{dN}{dE} = \sum_{i\ elements} A_i E^{-\gamma_i} e^{-\frac{E}{Z_i E_{cutoff}}}$$

A	Amplitude
γ	spectral index
E_{cutoff}	cut-off energy

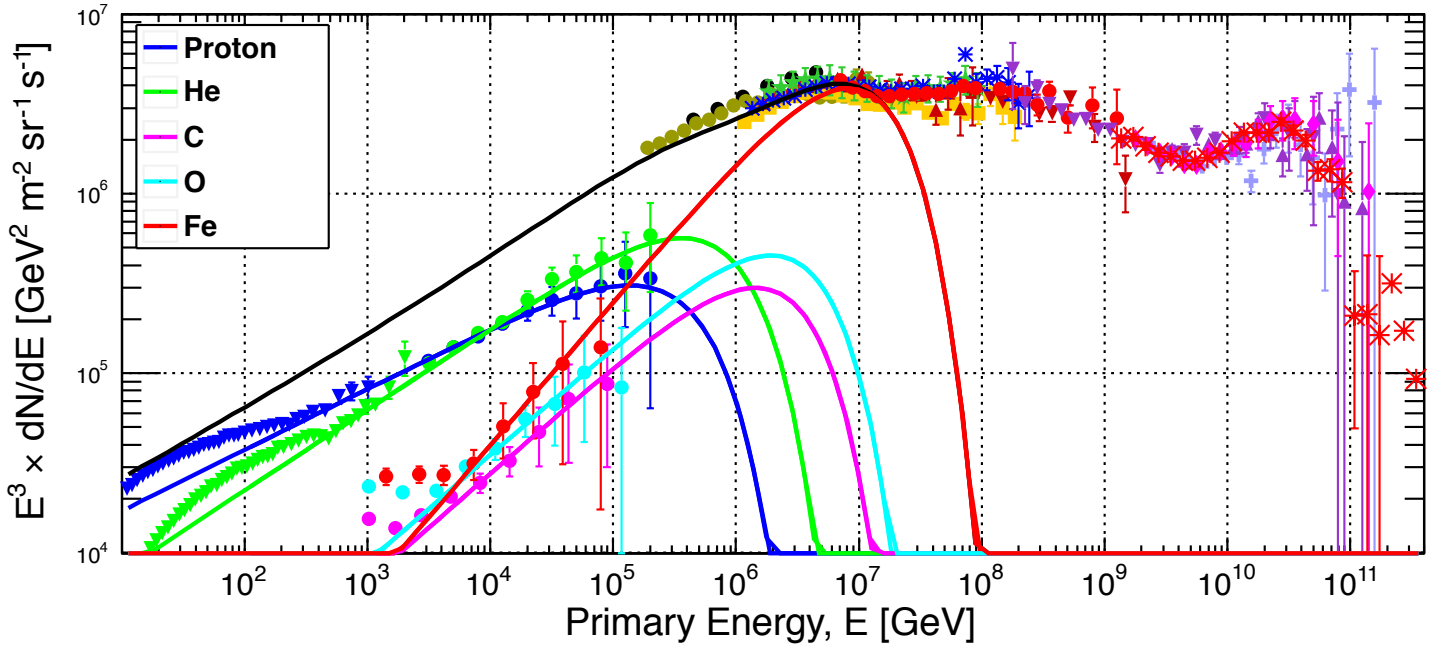

Amplitudes and indexes of all elements are defined by the CreamII data. Only the cutoffs need to be fit.

Fe spectrum is the key to the whole puzzle.

The Cream Fe data, when extended with the same index up to an energy where it makes 100% of the all particle spectrum, defines the maximum cut off energy for Fe.

This point turns out to be 26*400 TeV = 10.4 PeV.

This means proton cuts off at 400 TeV

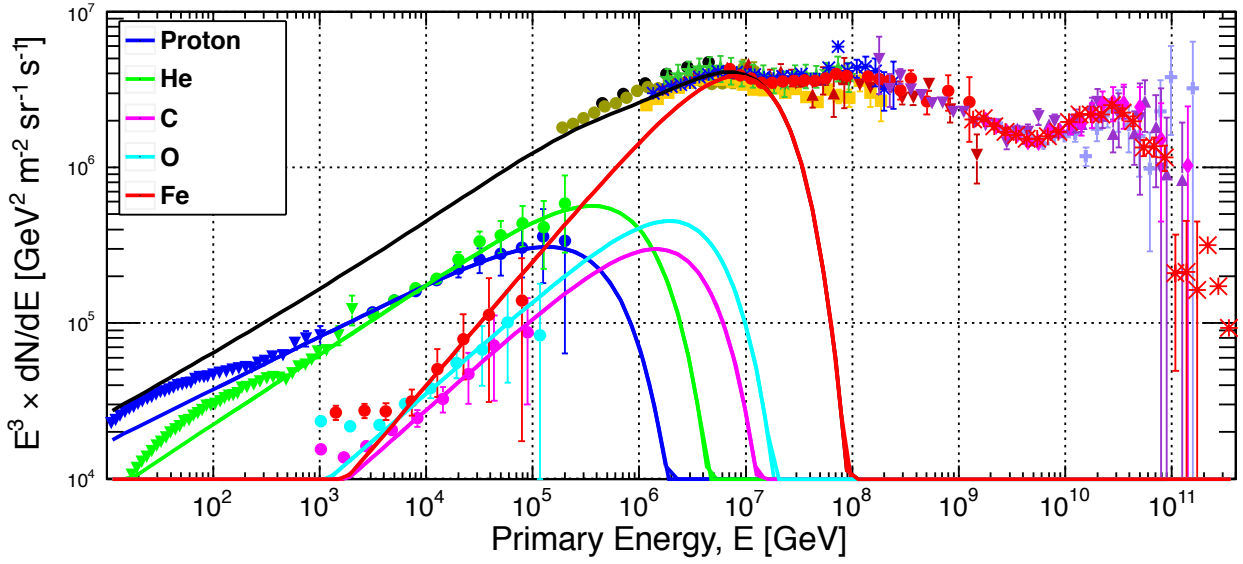

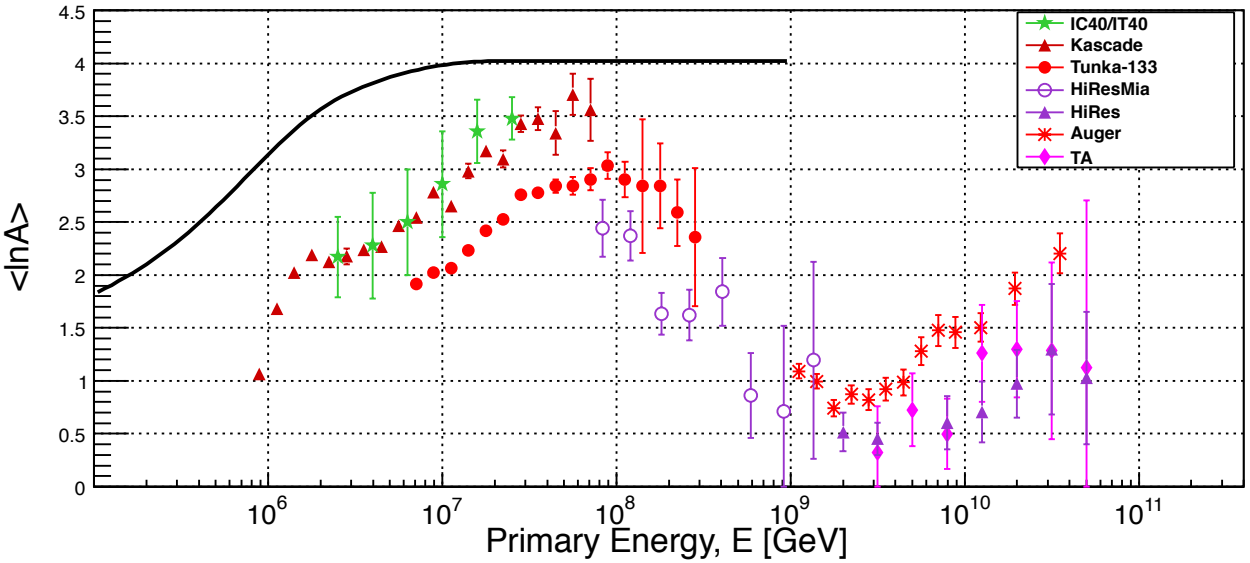

However

<lnA> data tells us
the knee is not 100% Fe.

Since the amplitudes are locked
by the Cream data,
the only way to fit <lnA> is
to bring the cutoff energy down

and fill the rest with light elements
of a new Peters cycle
(a new population of particles)

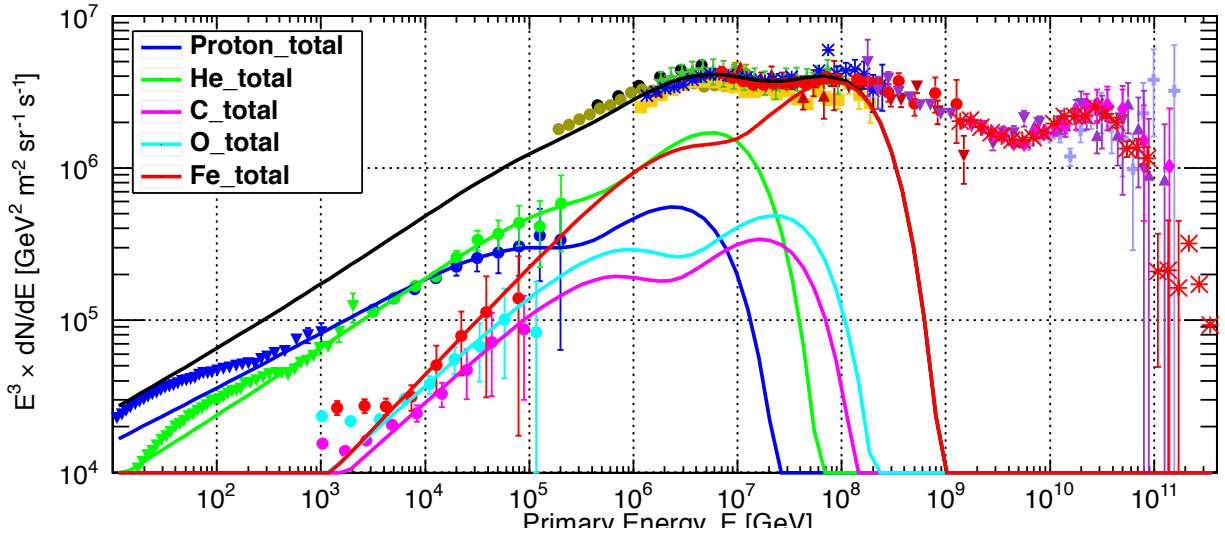

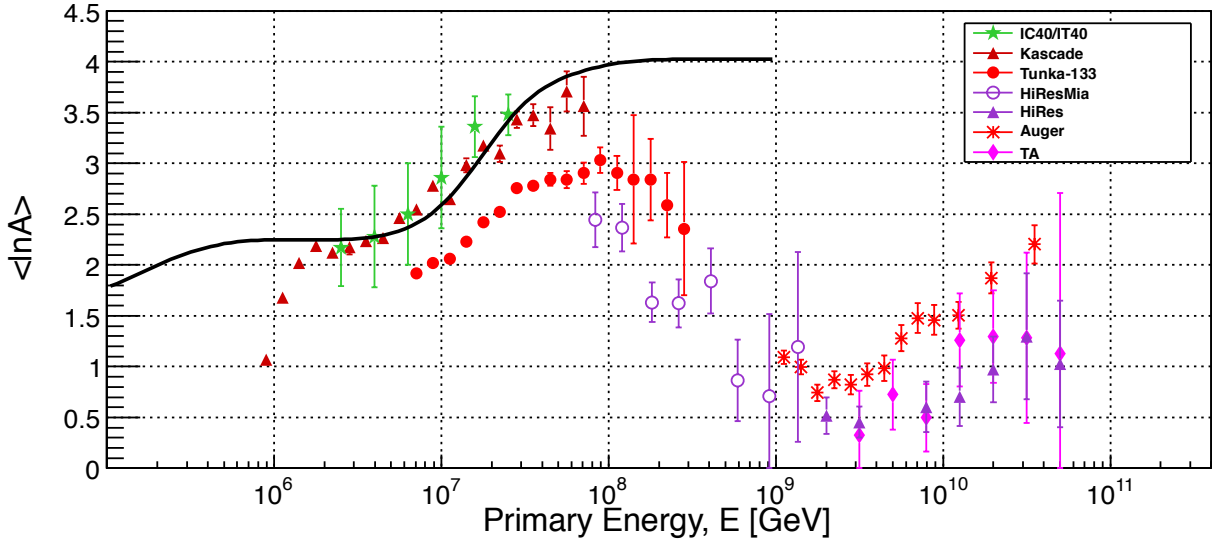

insert another Peter's cycle overlapping with the previous one until the best agreement with lnA is reached and constrained by the spectrum

$90\ \text{TeV} < E^{1}_{cutoff} < 150\ \text{TeV}$

and

$2\ \text{PeV} < E^{2}_{cutoff} < 4.5\ \text{PeV}$

with harder spectral indices

$\gamma_{Proton} = -2.4$

$\gamma_{He} = -2.3$

$\gamma_{CNO} = -2.3$

$\gamma_{Fe} = -2.2$

The comic ray knee is the intersection of two different source populations

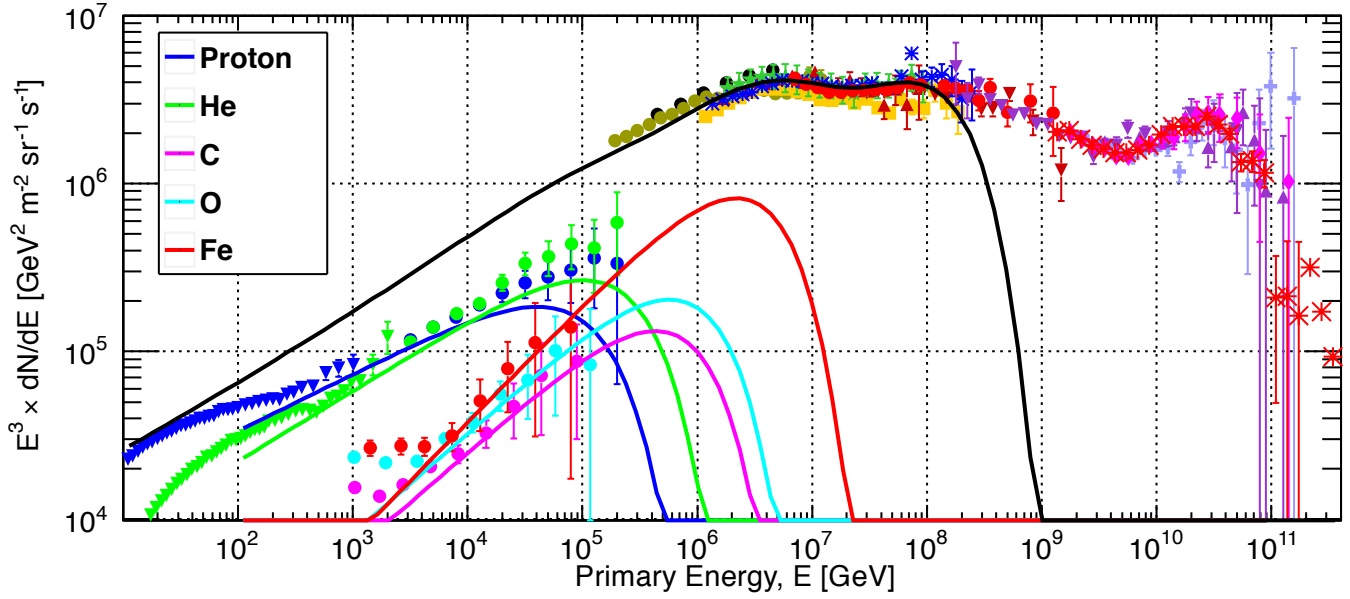

Population 1 alone

E^{p}_{cutoff} = 120 TeV

E^{Fe}_{cutoff} = *26 x* 120 TeV = 3.1 PeV

↓

The CR Knee

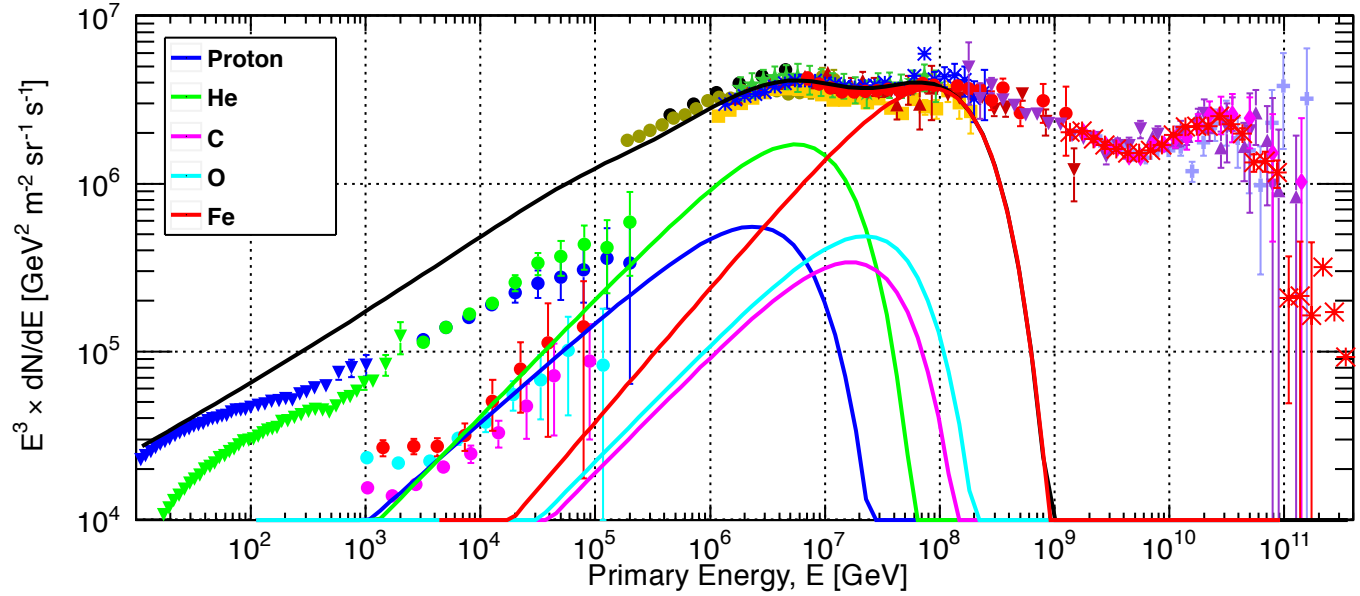

Population 2 alone

E^{p}_{cutoff} = 4 PeV

E^{Fe}_{cutoff} = *26 x* 4 TeV = 104 PeV

Proceed with the same method to inject another Peters cycle as Population 3

- The best fit is achieved with only Proton and Iron making up the spectrum, middle elements are reduced to negligible amounts.

- However, a gap is left between Pop2 and Pop3 and lnA turns to light too soon. There has to be some heavy elements at least upto 300 PeV.
  - ➔ include ultraheavy element groups as extension of Pop2 (as inspired by the lowE GCR measurements)

without ultraheavy nuclei

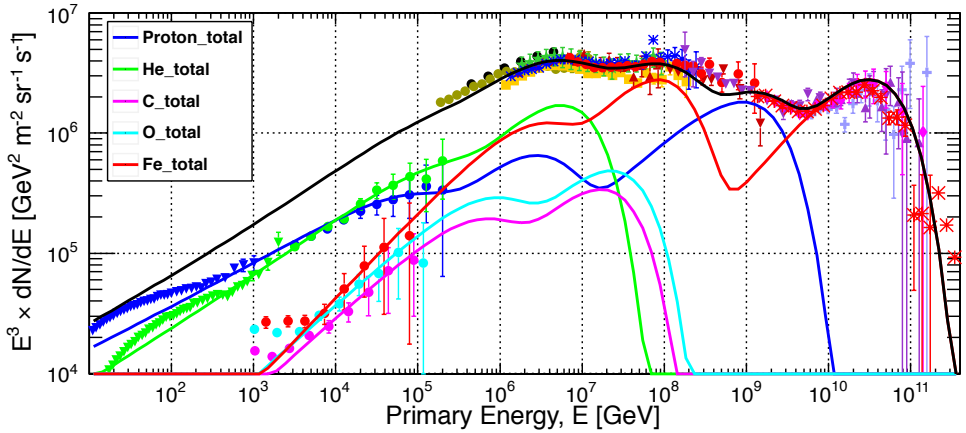

with ultraheavy nuclei

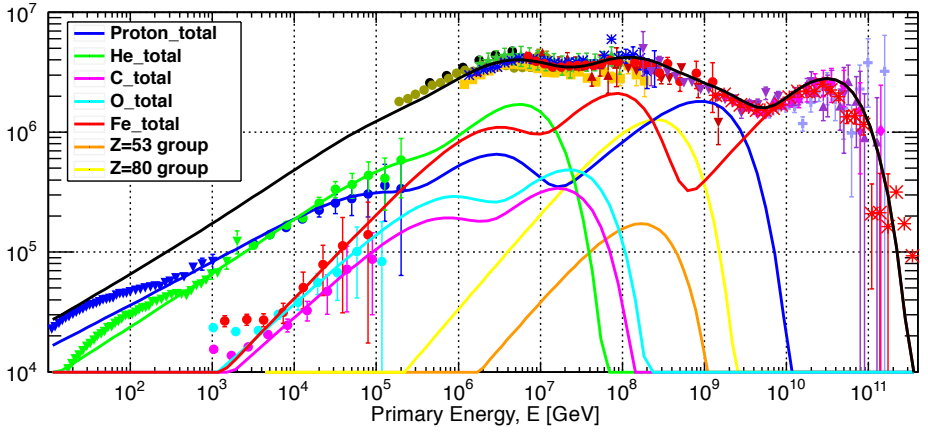

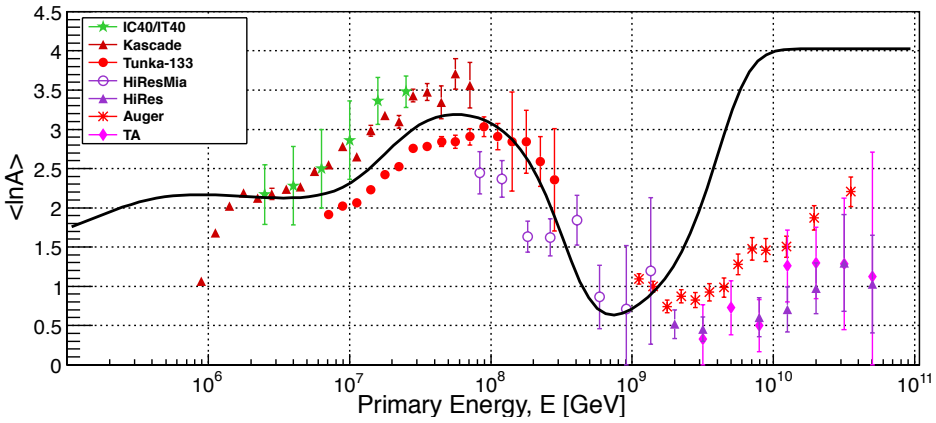

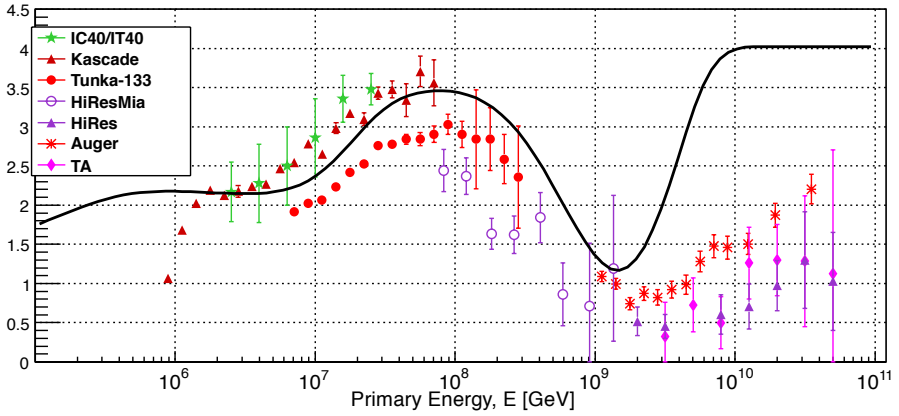

There has to be another proton under the Auger iron bump to bring <lnA> down

This extra proton has much harder spectrum with $E^{-2.2}$ and cuts off before Fe does

➔ extra-galactic proton cutting off due to GZK?

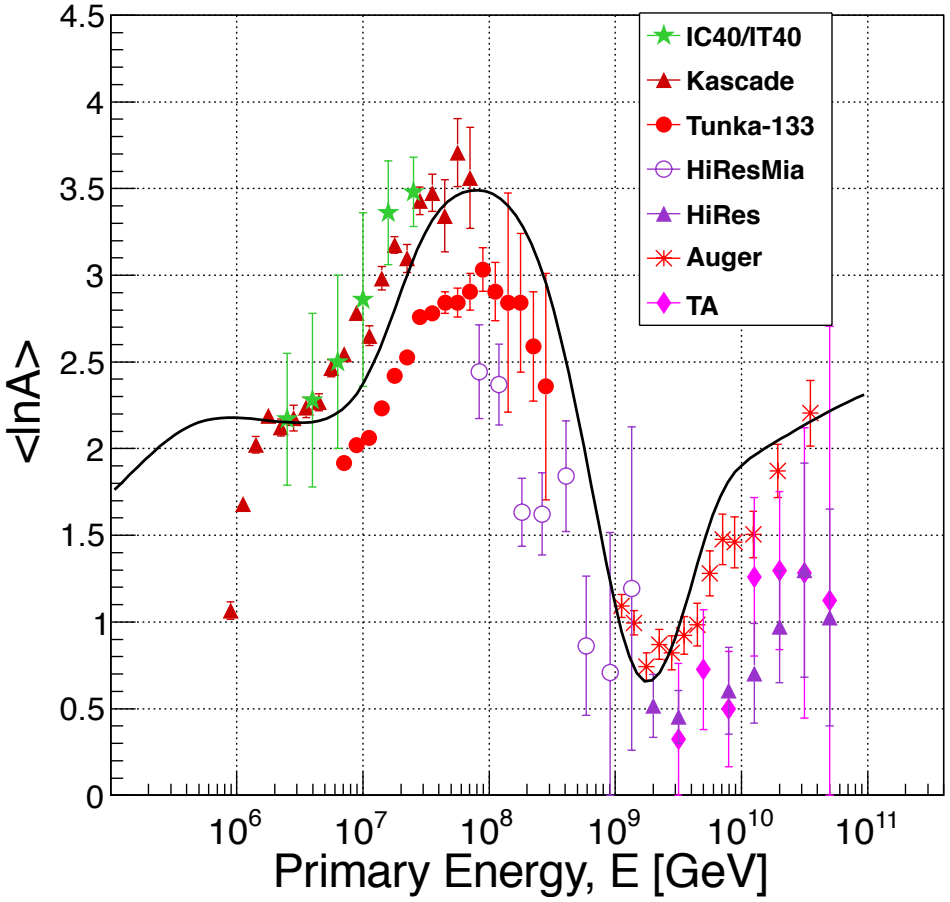

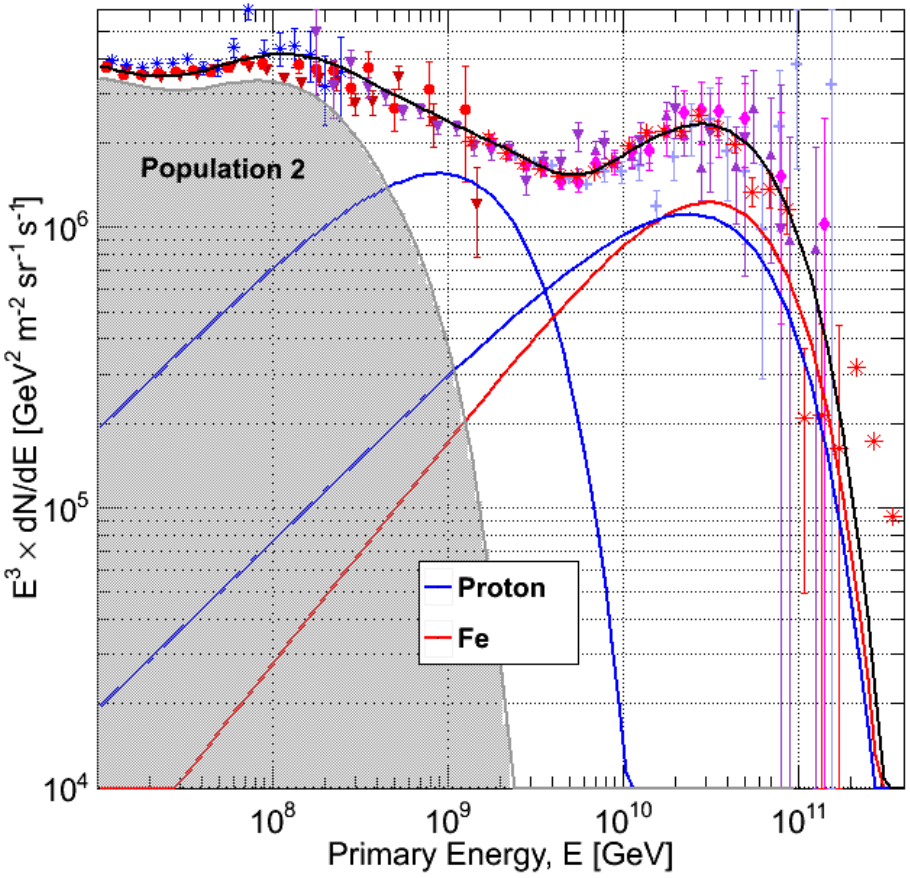

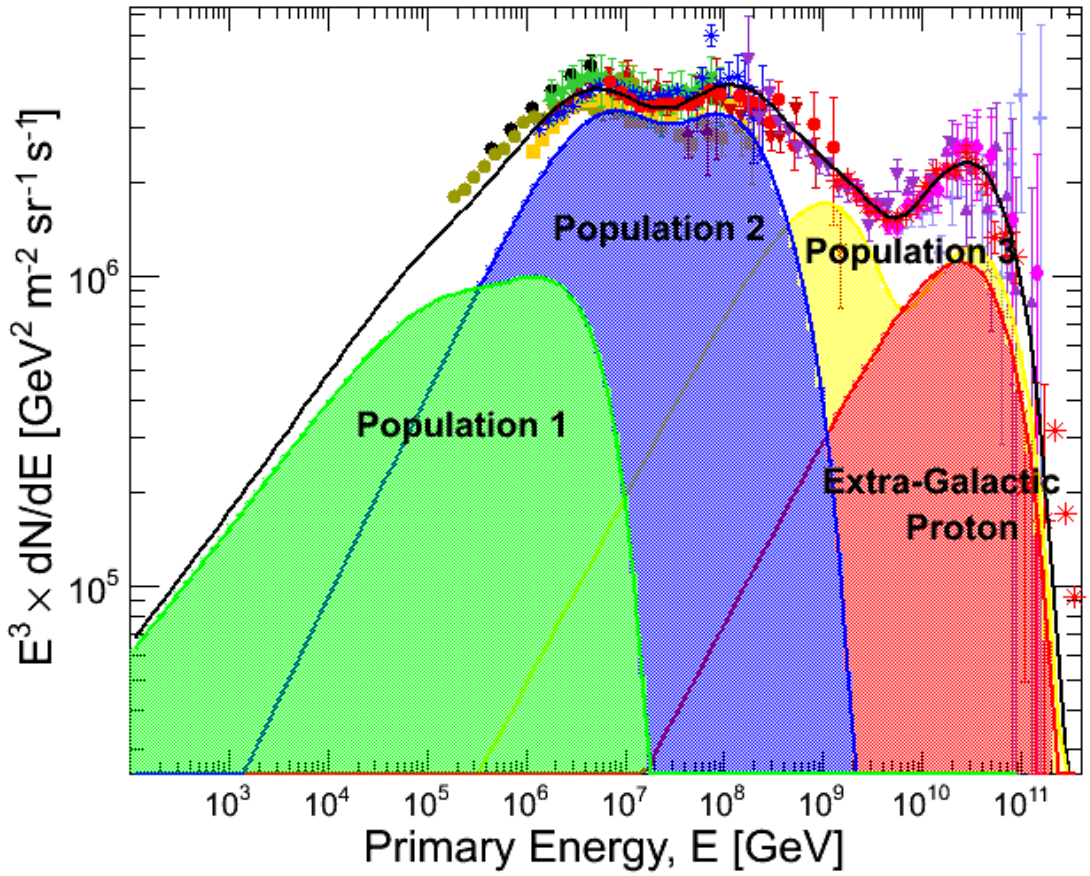

Population 1: The classical supernovae cutting around 100 TeV

Population 2: “Galactic PeVatron” ➔ TeV neutrinos

Population 3: “Galactic EeVatron” ➔ PeV neutrinos

Population 4: Extragalactic Proton: superposed on Population 3, cuts off due to GZK effect

◆ Spectral index of 2.7 is the superposition of much harder indices of different elements (e.g. Proton:2.4, middle nuclei:2.3, Fe:2.2)

Large Scale Anisotropy with IceCube / IceTop

IceCube
muon bundles > 1 TeV

IceTop
CR showers > 100 TeV

IceCube, ApJ 746, 33 (2012)

IceCube, ApJ 765, 55 (2013)

20 TeV

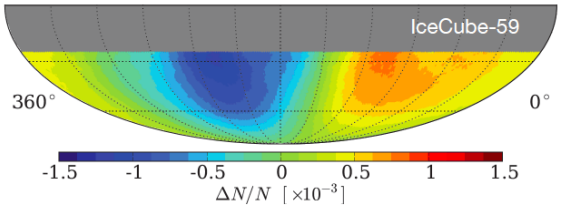

400 TeV

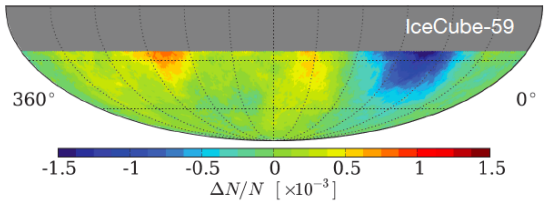

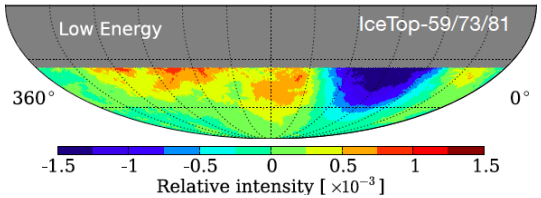

topology changes
between 20 - 400 TeV

anisotropy is not dipole

2 PeV

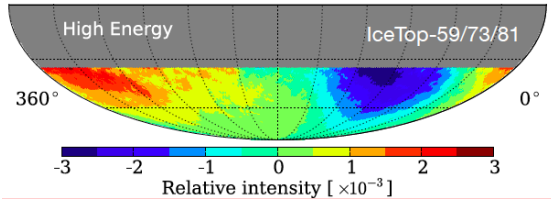

amplitude increases
with energy

10 PeV

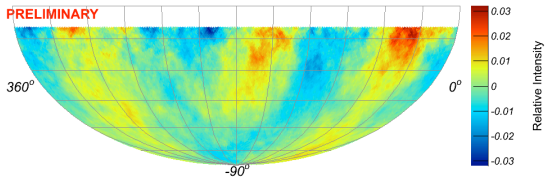

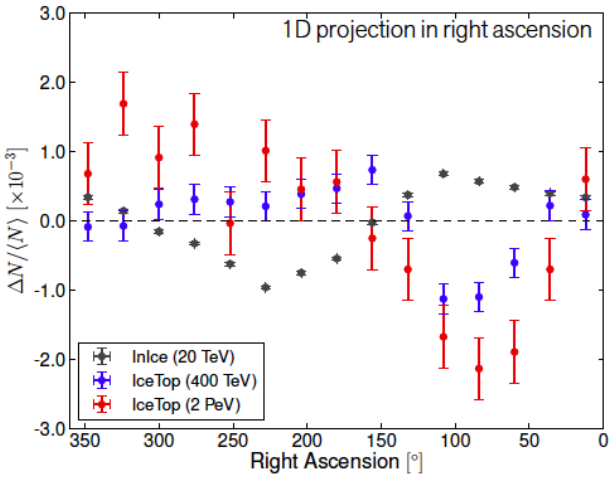

Search for large scale anisotropy: dipole analysis

I. Sidelnik,
R. de Almeida
ICRC 2013

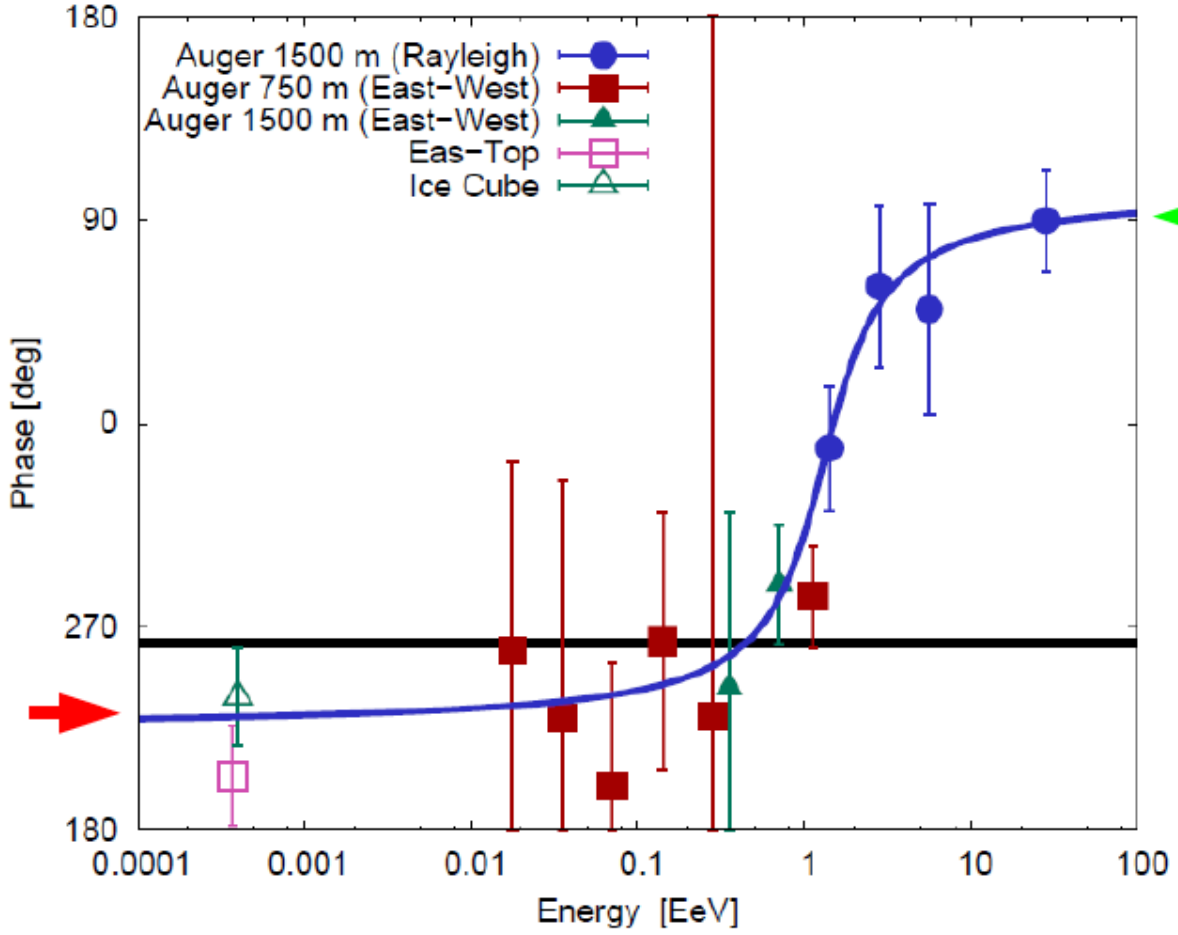

Hints for dipole in data

- Amplitude not significant...
- ...yet phase shows interesting transition

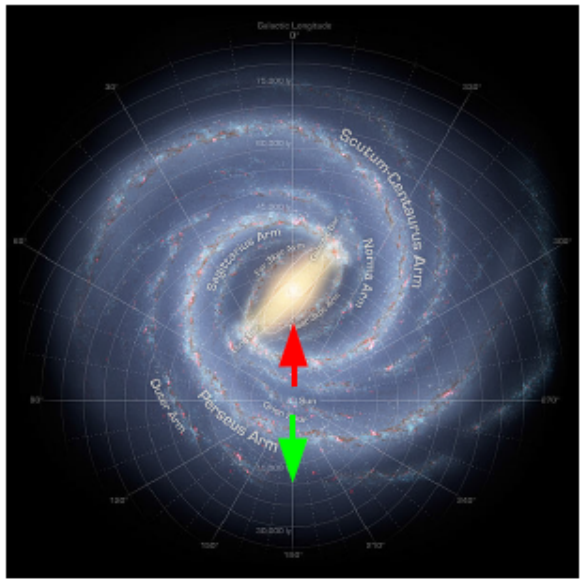

Prescription running since 25 June 2011 to confirm result with 99 % confidence

Eas-Top: M. Aglietta *et al.* 2009 ApJ **692** L130
IceCube: R. Abbasi *et al.* 2012 ApJ **746** 33

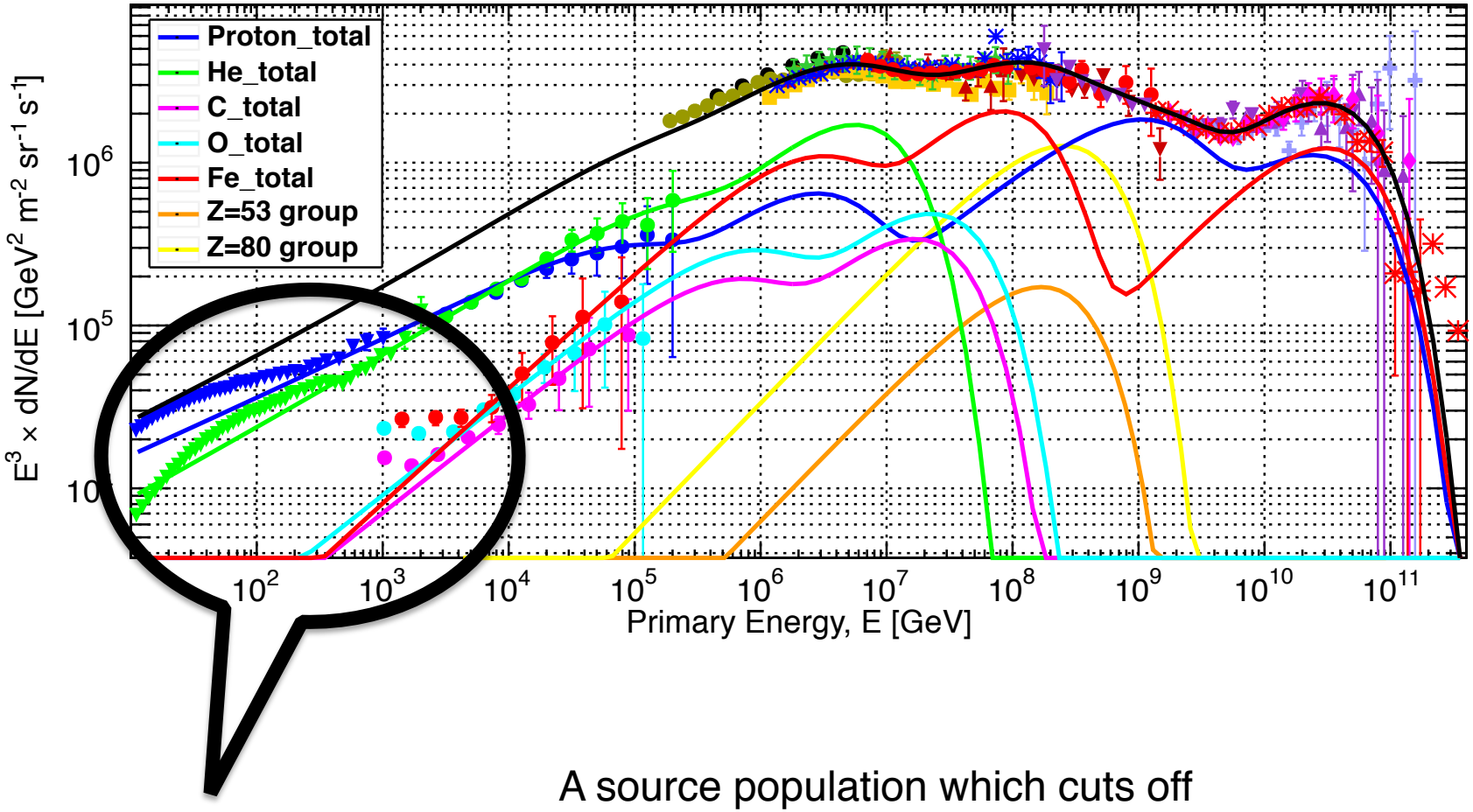

There is yet another Peter's cycle here

A source population which cuts off around 100 GeV will explain the PAMELA break, which is the overlap between this population and the harder classic supernovae component setting in.

FERMI-LAT

SCIENCE VOL 339 15 FEBRUARY 2013

Detection of the Characteristic Pion-Decay Signature in Supernova Remnants

M. Ackermann,[1] M. Ajello,[2] A. Allafort,[3] L. Baldini,[4] J. Ballet,[5] G. Barbiellini,[6,7] M. G. Baring,[8] D. Bastieri,[9,10] K. Bechtol,[3] R. Bellazzini,[11] R. D. Blandford,[3] E. D. Bloom,[3] E. Bonamente,[12,13] A. W. Borgland,[3] E. Bottacini,[3] T. J. Brandt,[14] J. Bregeon,[11] M. Brigida,[15,16] P. Bruel,[17] R. Buehler,[3] G. Busetto,[9,10] S. Buson,[9,10] G. A. Caliandro,[18] R. A. Cameron,[3] P. A. Caraveo,[19] J. M. Casandjian,[5] C. Cecchi,[12,13] Ö. Çelik,[14,20,21] E. Charles,[3] S. Chaty,[5] R. C. G. Chaves,[5] A. Chekhtman,[22] C. C. Cheung,[23] J. Chiang,[3] G. Chiaro,[24] A. N. Cillis,[14,25] S. Ciprini,[13,26] R. Claus,[3] J. Cohen-Tanugi,[27] L. R. Cominsky,[28] J. Conrad,[29,30,31] S. Corbel,[5,32] S. Cutini,[33] F. D'Ammando,[12,34,35] A. de Angelis,[36] F. de Palma,[15,16] C. D. Dermer,[37] E. do Couto e Silva,[3] P. S. Drell,[3] A. Drlica-Wagner,[3] L. Falletti,[27] C. Favuzzi,[15,16] E. C. Ferrara,[14] A. Franckowiak,[3] Y. Fukazawa,[38] S. Funk,[3]* P. Fusco,[15,16] F. Gargano,[16] S. Germani,[12,13] N. Giglietto,[15,16] P. Giommi,[33] F. Giordano,[15,16] M. Giroletti,[39] T. Glanzman,[3] G. Godfrey,[3] I. A. Grenier,[5] M.-H. Grondin,[40,41] J. E. Grove,[37] S. Guiriec,[14] D. Hadasch,[18] Y. Hanabata,[38] A. K. Harding,[14] M. Hayashida,[3,42] K. Hayashi,[38] E. Hays,[14] J. W. Hewitt,[14] A. B. Hill,[3,43] R. E. Hughes,[44] M. S. Jackson,[30,45] T. Jogler,[3] G. Jóhannesson,[46] A. S. Johnson,[3] T. Kamae,[3] J. Kataoka,[47] J. Katsuta,[3] J. Knödlseder,[48,49] M. Kuss,[11] J. Lande,[3] S. Larsson,[29,30,50] L. Latronico,[51] M. Lemoine-Goumard,[52,53] F. Longo,[6,7] F. Loparco,[15,16] M. N. Lovellette,[37] P. Lubrano,[12,13] G. M. Madejski,[3] F. Massaro,[3] M. Mayer,[1] M. N. Mazziotta,[16] J. E. McEnery,[14,54] J. Mehault,[27] P. F. Michelson,[3] R. P. Mignani,[55] W. Mitthumsiri,[3] T. Mizuno,[56] A. A. Moiseev,[20,54] M. E. Monzani,[3] A. Morselli,[57] I. V. Moskalenko,[3] S. Murgia,[3] T. Nakamori,[47] R. Nemmen,[14] E. Nuss,[27] M. Ohno,[58] T. Ohsugi,[56] N. Omodei,[3] M. Orienti,[39] E. Orlando,[3] J. F. Ormes,[59] D. Paneque,[3,60] J. S. Perkins,[14,21,20,61] M. Pesce-Rollins,[11] F. Piron,[27] G. Pivato,[10] S. Rainò,[15,16] R. Rando,[9,10] M. Razzano,[11,62] S. Razzaque,[22] A. Reimer,[3,63] O. Reimer,[3,63] S. Ritz,[62] C. Romoli,[10] M. Sánchez-Conde,[3] A. Schulz,[1] C. Sgrò,[11] P. E. Simeon,[3] E. J. Siskind,[64] D. A. Smith,[52] G. Spandre,[11] P. Spinelli,[15,16] F. W. Stecker,[14,65] A. W. Strong,[66] D. J. Suson,[67] H. Tajima,[3,68] H. Takahashi,[38] T. Takahashi,[58] T. Tanaka,[3,69]* J. G. Thayer,[3] J. B. Thayer,[3] D. J. Thompson,[14] S. E. Thorsett,[70] L. Tibaldo,[9,10] O. Tibolla,[71] M. Tinivella,[11] E. Troja,[14,72] Y. Uchiyama,[3]* T. L. Usher,[3] J. Vandenbroucke,[3] V. Vasileiou,[27] G. Vianello,[3,73] V. Vitale,[57,74] A. P. Waite,[3] M. Werner,[63] B. L. Winer,[44] K. S. Wood,[37] M. Wood,[3] R. Yamazaki,[75] Z. Yang,[29,30] S. Zimmer[29,30]

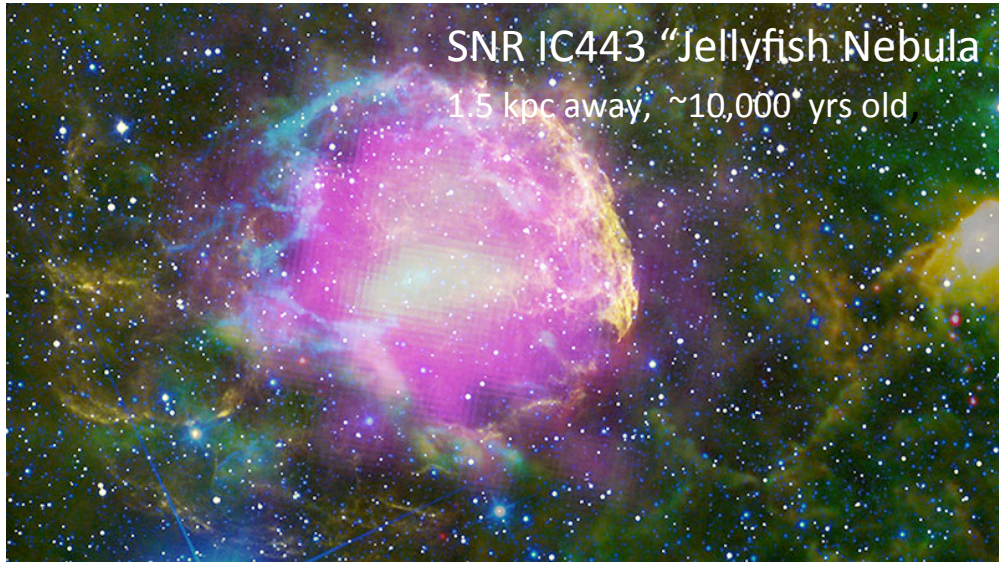

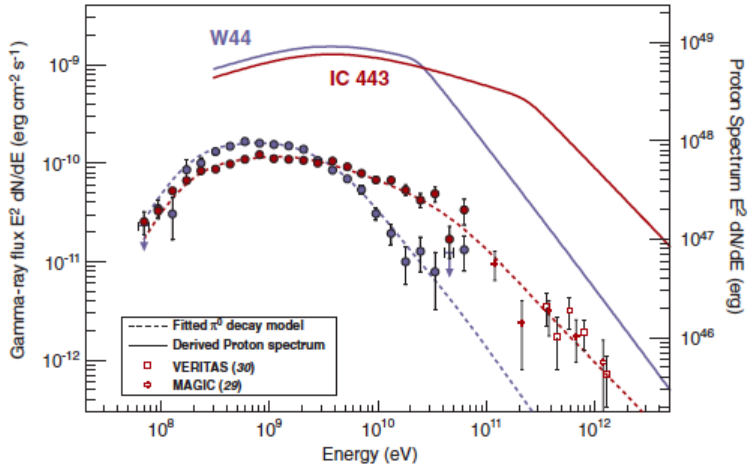

Fig. 3. Proton and gamma-ray spectra determined for IC 443 and W44. Also shown are the broadband spectral flux points derived in this study, along with TeV spectral data points for IC 443 from MAGIC (*29*) and VERITAS (*30*). The curvature evident in the proton distribution at ~2 GeV is a consequence of the display in energy space (rather than momentum space). Gamma-ray spectra from the protons were computed using the energy-dependent cross section parameterized by (*32*). We took into account accelerated nuclei (heavier than protons) as well as nuclei in the target gas by applying an enhancement factor of 1.85 (*33*). Note that models of the gamma-ray production via *pp* interactions have some uncertainty. Relative to the model adopted here, an alternative model of (*6*) predicts ~30% less photon flux near 70 MeV; the two models agree with each other to better than 15% above 200 MeV. The proton spectra assume average gas densities of n = 20 cm^{-3} (IC 443) and n = 100 cm^{-3} (W44) and distances of 1.5 kpc (IC 443) and 2.9 kpc (W44).

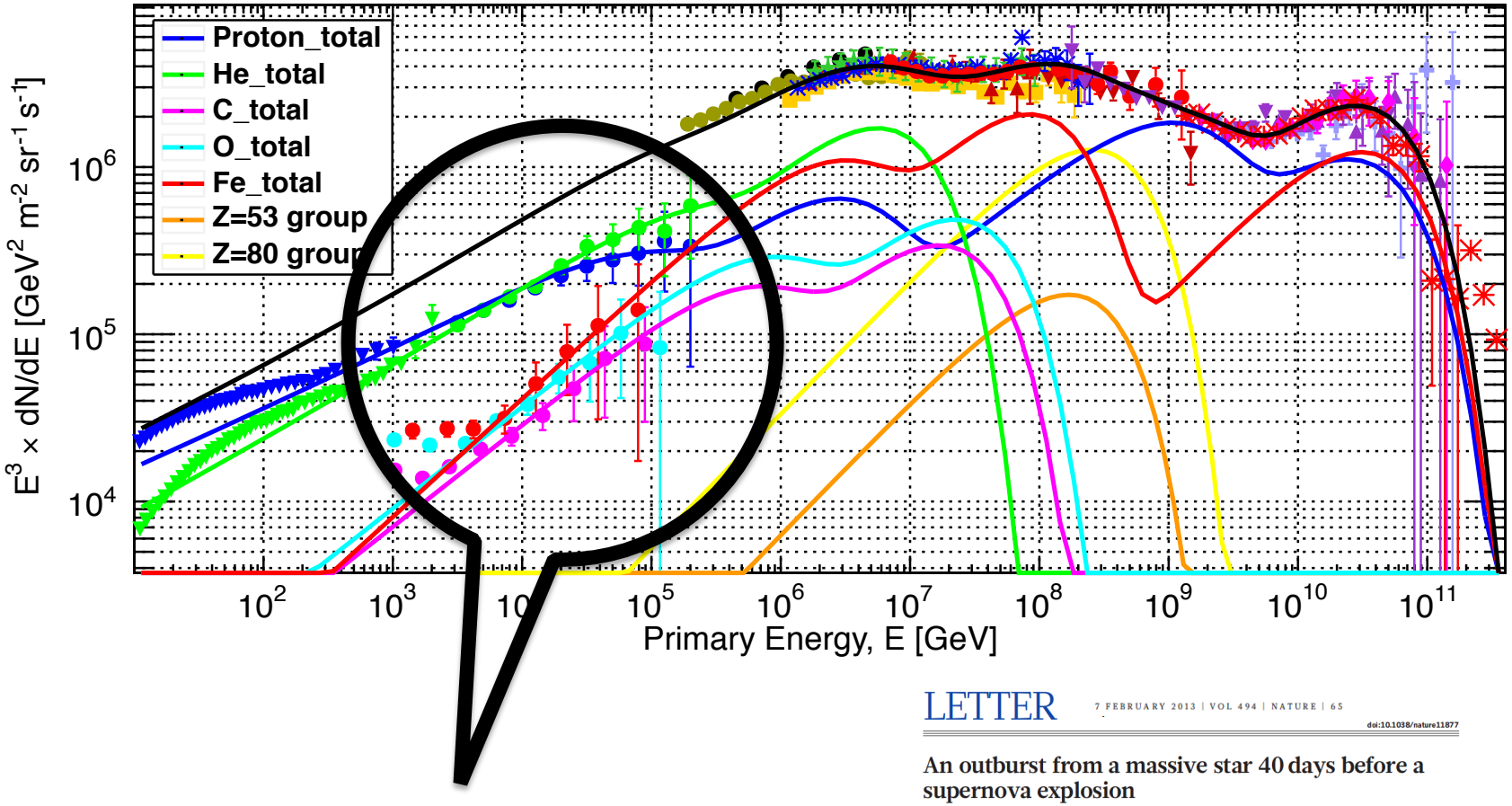

The classical supernovae cutting around 100 TeV

Massive stars, circumstellar ejecta

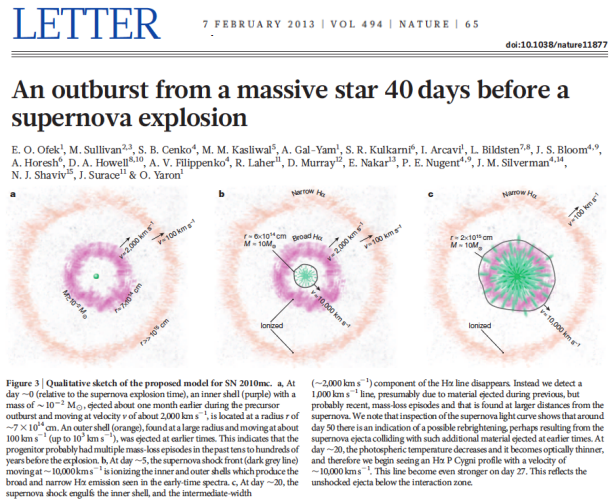

LETTER 7 FEBRUARY 2013 | VOL 494 | NATURE | 65

doi:10.1038/nature11877

An outburst from a massive star 40 days before a supernova explosion

E. O. Ofek[1], M. Sullivan[2,3], S. B. Cenko[4], M. M. Kasliwal[5], A. Gal-Yam[1], S. R. Kulkarni[6], I. Arcavi[1], L. Bildsten[7,8], J. S. Bloom[4,9], A. Horesh[6], D. A. Howell[8,10], A. V. Filippenko[4], R. Laher[11], D. Murray[12], E. Nakar[13], P. E. Nugent[4,9], J. M. Silverman[4,14], N. J. Shaviv[15], J. Surace[11] & O. Yaron[1]

Figure 3 | Qualitative sketch of the proposed model for SN 2010mc. a, At day ~0 (relative to the supernova explosion time), an inner shell (purple) with a mass of ~10^{-2} $M_{\odot}$, ejected about one month earlier during the precursor outburst and moving at velocity v of about 2,000 km s^{-1}, is located at a radius r of ~7×10^{14} cm. An outer shell (orange), found at a large radius and moving at about 100 km s^{-1} (up to 10^3 km s^{-1}), was ejected at earlier times. This indicates that the progenitor probably had multiple mass-loss episodes in the past tens to hundreds of years before the explosion. b, At day ~5, the supernova shock front (dark grey line) moving at ~10,000 km s^{-1} is ionizing the inner and outer shells which produce the broad and narrow Hα emission seen in the early-time spectra. c, At day ~20, the supernova shock engulfs the inner shell, and the intermediate-width (~2,000 km s^{-1}) component of the Hα line disappears. Instead we detect a 1,000 km s^{-1} line, presumably due to material ejected during previous, but probably recent, mass-loss episodes and that is found at larger distances from the supernova. We note that inspection of the supernova light curve shows that around day 50 there is an indication of a possible rebrightening, perhaps resulting from the supernova ejecta colliding with such additional material ejected at earlier times. At day ~20, the photospheric temperature decreases and it becomes optically thinner, and therefore we begin seeing an Hα P Cygni profile with a velocity of ~10,000 km s^{-1}. This line become even stronger on day 27. This reflects the unshocked ejecta below the interaction zone.

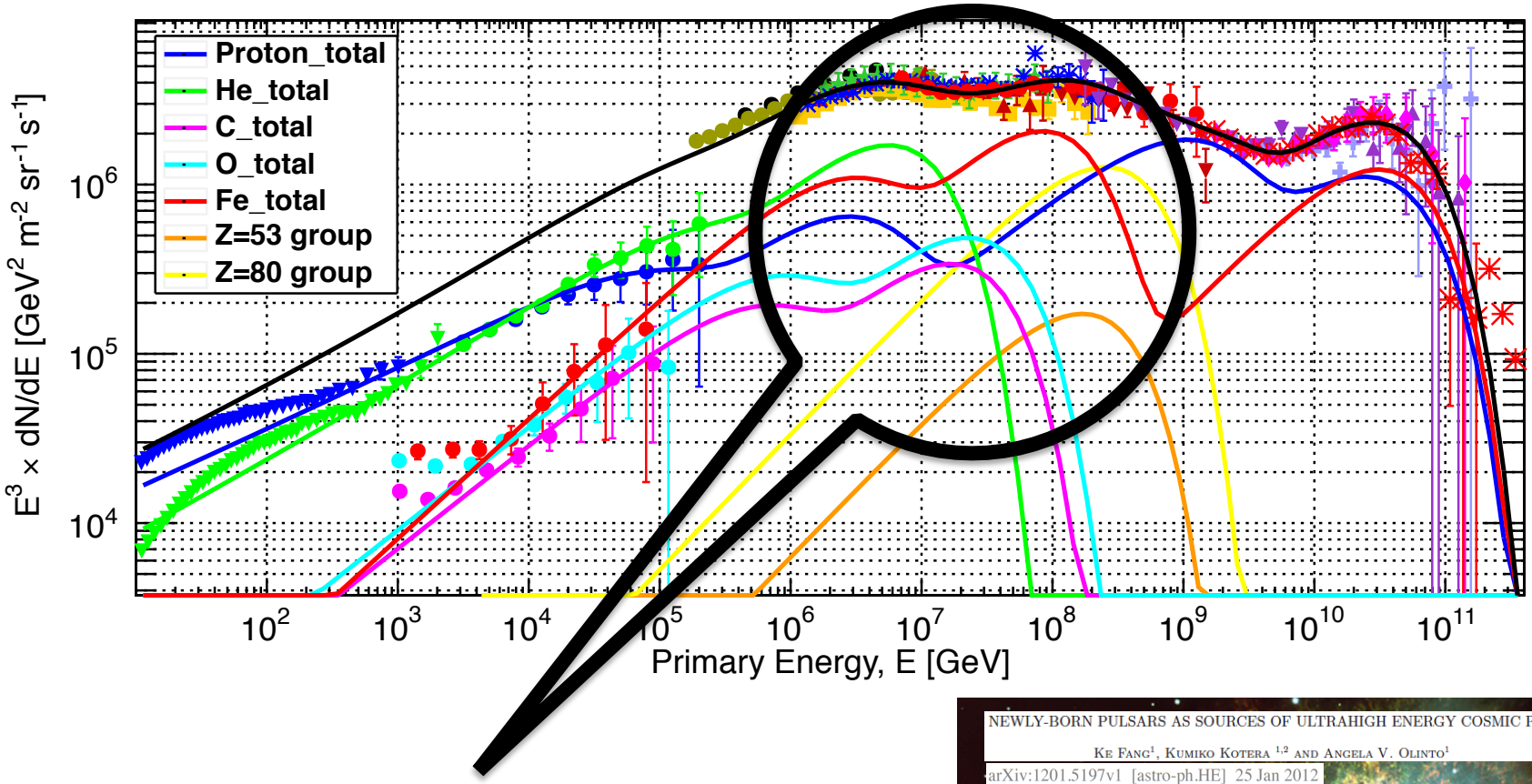

Fast spinning more massive stars

beamed structure

➔ Pulsar Wind Nebula systems

Observation of High-Energy Astrophysical Neutrinos in Three Years of IceCube Data

arXiv:1405.5303v2 [astro-ph.HE] 2 Jul 2014

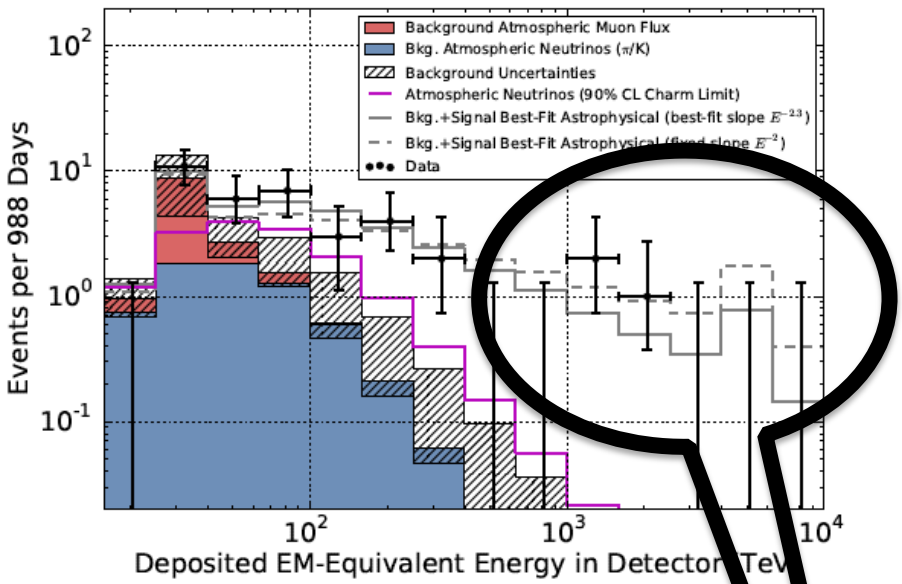

FIG. 2. Deposited energies of observed events with predictions. The hashed region shows uncertainties on the sum of all backgrounds. Muons (red) are computed from simulation to overcome statistical limitations in our background measurement and scaled to match the total measured background rate. Atmospheric neutrinos and uncertainties thereon are derived from previous measurements of both the π/K and charm components of the atmospheric ν_μ spectrum [9]. A gap larger than the one between 400 and 1000 TeV appears in 43% of realizations of the best-fit continuous spectrum.

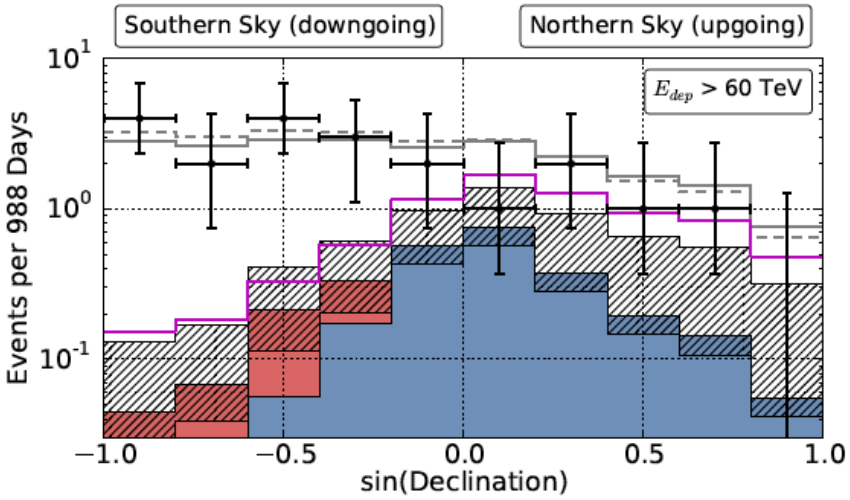

FIG. 3. Arrival angles of events with $E_{dep} > 60$ TeV, as used in our fit and above the majority of the cosmic ray muon background. The increasing opacity of the Earth to high energy neutrinos is visible at the right of the plot. Vetoing atmospheric neutrinos by muons from their parent air showers depresses the atmospheric neutrino background on the left. The data are described well by the expected backgrounds and a hard astrophysical isotropic neutrino flux (gray lines). Colors as in Fig. 2. Variations of this figure with other energy thresholds are in the online supplement [29].

1-2 PeV neutrinos as secondaries will come from ~ 20-40 PeV region of CR spectrum

6 source populations explain the observed CR spectrum and <lnA>

Source 1: The Sun (cutting off around 10 GeV)

Population 2: Old SNR (~10-20 kyrs old, e.g. IC443, W44, W28), cuts off ~100GeV

Population 3: The classical supernova cutting off around 100 TeV, ~1-3 in 100 yrs
Massive stars, circumstellar ejecta

Population 4: "Galactic PeVatron": PWN/Hypernovae, 1 in 1000 yrs ➔ TeV –PeV neutrinos
Fast spinning massive stars with mass 20-50 $M_{sun,}$ beamed structure
found in star forming regions, live wild, die young,
leave a fast spinning pulsar behind

Population 5: "Galactic EeVatron": Hypernovae/GRB, 1 in 10000 yrs ➔ PeV neutrinos

Population 6: extragalactic Proton: superposed on population 5 ➔ PeV neutrinos

IceCube's TeV-PeV neutrinos are a mixture of Pop4 + Pop5 + Pop6 (galactic + extragalactic)